Environmental Science and Pollution Research (2019) 26:9672–9685
https://doi.org/10.1007/s11356-019-04277-0

RESEARCH ARTICLE

Enhanced performance of alkali-modified $Bi_2WO_6/Bi_{0.15}Ti_{0.85}O_2$ toward photocatalytic oxidation of HCHO under visible light

Qiong Huang[1] · Juan Ye[1] · Han Si[1] · Jiaxin Ruan[1] · Mengxin Xu[1] · Bo Yang[1] · Tao Tao[1] · Yunxia Zhao[1] · Mindong Chen[1]

Received: 29 October 2018 / Accepted: 16 January 2019 / Published online: 7 February 2019

Abstract

Photocatalytic oxidation of formaldehyde (HCHO) is considered as one of the promising ways to resolve indoor air HCHO pollution. TiO_2 has been well known as the most extended application in photocatalysis due to its strong oxidizing ability and stability. Owing to high activity under visible light irradiation, TiO_2 and Bi_2O_3 doping mixed with Bi_2WO_6 was analyzed in this study. The formation of two kinds of heterojunction caused efficient charge separation, leading to the effective reduction in the recombination of photo-generated electron and hole. The special structure and enhanced performance of these catalysts were analyzed. For the first time, the loading of alkali salts was researched for photocatalytic oxidation. In order to understand the reaction mechanism of alkali salts enhanced effects, the catalysts were investigated by using BET, XRD, UV–Vis, FT-IR, SEM, and XPS. The results found more than 2 wt% of Na_2SO_4 loading and the mixed methods with different solutions were key factors affecting the performance of catalysts. Nearly 92% HCHO conversion could be completed over $Bi_2WO_6/Bi_{0.15}Ti_{0.85}O_2$ (Na_2SO_4), and the concentration of HCHO was only 0.07 mg/m^3 for 24 h, which was below the limit of specification in China. The results also indicated that the solution mixing method was more favorable to increase the HCHO conversion due to decrease the size of $Bi_{0.15}T_{i0.85}O_2$ particles. The catalysts with Na_2SO_4 loading provided more surface-adsorbed oxygen that facilitated the desorption of CO_2 and markedly increased the photocatalytic oxidation of HCHO.

Keywords Photocatalytic oxidation · HCHO · Catalysts · Alkali-modification · Visible light · Air pollution

Research highlights

1. The structure and performance of different $Bi_2WO_6/Bi_{0.15}Ti_{0.85}O_2$ catalysts were discussed in details and understand the strong interaction.
2. The reason for the liquid combining method instead of by the mechanism mixing that showed more favorable for HCHO conversion could be interpreted.
3. A possible photocatalytic mechanism for HCHO oxidation over these catalysts is proposed to interpret the increased activity.
4. The effect of alkali salts, especially for Na_2SO_4 for the increased activity for HCHO oxidation, can be discussed and explained by XPS and FT-IR.

Responsible editor: Suresh Pillai

✉ Qiong Huang
hqhaixia@163.com

[1] Jiangsu Collaborative Innovation Center of Atmospheric Environment and Equipment Technologies, Jiangsu Key Laboratory of Atmospheric Environmental Monitoring and Pollution Control, School of Environmental Science and Engineering, Nanjing University of Information Science and Technology, No. 219 Ningliu Road, Nanjing 210044, China

Introduction

Volatile organic compounds (VOCs) have been identified as the potential environmental pollutants due to their strong toxicity to the environment (Sanz et al. 2011; Topka et al. 2016), particularly in developing countries (Yang 2014; Yang et al. 2018a). Among VOCs, formaldehyde (HCHO) is a kind of major indoor air pollutant and longtime exposure of high concentration HCHO may lead to health damages (Portela et al. 2017; Yang et al. 2000; Yang et al. 2018b). Photocatalytic oxidation is considered as one of the promising ways to remove HCHO due to its advantages of visible light reaction and energy-saving (Zhu et al. 2018). TiO_2, as one of the important semiconductor materials, has been known as the most extended application in photocatalysis, and it has been proverbially considered due to its strong oxidizing ability, non-toxic, and stable structure (Hwang et al. 2017). Recently, an unusual strong absorption band spanning the full spectrum of visible light has been accomplished in anatase TiO_2 by introducing atomic hydrogen-mediated oxygen vacancies (Yang et al.

2018c), which cause active photo-electrochemical water oxidation in visible light. Some researchers focused on the recent development of modified TiO_2 used for degrading gas phase pollutants under ambient temperature (Shayegan et al. 2018). Modification techniques, such as metal and non-metal doping, co-doping, and the heterojunction of TiO_2 with other semiconductors, have also been developed. Meantime, lots of efforts have been investigated to improve the activity and extend the absorption band into the visible region. In particular, an enormous amount of researches worked on the regulation of TiO_2 with metal, non-metal, or other as organic photosensitizers (Lucky et al. 2010; Mattsson et al. 2013; Wang et al. 2012). Owing to the narrow energy gap, Bi_2O_3 doping has been demonstrated to be one of the effective ways to get a high activity under visible light irradiation (Hu et al. 2012; Liu et al. 2010), while Zhang et al. (2018) reported that Bi/Bi_2O_3 showed much higher efficiency as compared to bare Bi_2O_3, which may be attributed to the synergistic effects of porous structures, improved optical absorption, and surface plasmon resonance. One research exhibited that the structure of mixed TiO_2 and Bi_2O_3 was heterojunction state (Huang et al. 2017), which may be beneficial to improve the activity, owing to enhance the separation of photo-generated electrons and holes, and decrease the recombination with electron transformation. But this tiny Bi_2O_3 could be easily subjected to phase transformation and lead to poor stability (Zhu et al. 2011). Recently, the structure and morphology of photocatalysts have attracted enormous attention due to the absorption of organic compounds and visible light.

Bismuth oxides (He et al., 2018a, b; Huang et al. 2016; Li et al. 2015), as one of the photocatalysts, have received more attention owing to individual structure and high photocorrosion stabilization. Among of them, pure Bi_2WO_6 was considered as a perfect photocatalyst in the application of photocatalytic oxidation under visible light (Wang et al. 2014). In general, the material structure is one of the most important factors to affect the activity of catalysts. Meanwhile, a great number of the different structures of Bi_2WO_6, such as nanoplates, nanosheet, microsphere, and flower-like (Cui et al. 2016; Wang et al. 2013; Zhang et al. 2015), have been synthesized to increase the activity and stability. However, the performance of Bi_2WO_6 is usually restricted by the poor absorption of light, slow rate of charge transfer, and the high recombination of photo-generated electrons and holes (Xia et al. 2014). Therefore, some of the strategies have been used to further improve the performance of Bi_2WO_6. Just as TiO_2, some of the metal or non-metal materials were appended in order to improve the visible light response (Tian et al. 2014; Wang et al. 2018; Yan et al. 2018). However, the thermal stability of the ions could be decreased and the ions turned into the recombination centers of photo-generated electron and hole (Tian et al. 2013). In addition, these surface defects on the reactive surface could be formed and change photocatalytic activities due to strongly affect its chemical and electronic structure (Liu et al. 2015). More importantly, the formation of heterojunction states, such as g-C_3N_4/TiO_2 (Low et al. 2017), Bi_2O_3/g-C_3N_4 (He et al., 2018a, b), $BiOI/TiO_2$ (Li et al. 2018), β-Bi_2O_3@Bi_2S_3 (Yu et al. 2018), BiOI@La $(OH)_3$ (Sun et al. 2017), Bi_2WO_6@Bi_2S_3 (Huang et al., 2018a, b), $BiVO_4$/g-C_3N_4 (Cui et al. 2018), and Bi_2O_3NPs/ZnMeLDH (Me=Al, Cr) (Carja et al. 2018), have been confirmed as a fascinating way for improving the activities owing to amplify the absorption range of light and enhance the efficiency of charge separation. Therefore, the combination of Bi_2WO_6 and TiO_2 with Bi_2O_3 doping could be a peculiar strategy to improve the photocatalytic activity and efficiency. To the best of our knowledge, synthesized Bi_2WO_6/Bi-TiO_2 heterostructure photocatalysts and the performances with visible light irradiation have not been reported.

Recently, it is widely recognized that alkali modification of catalysts is an effective method to enhance the activity for HCHO and CO oxidation. For instance, the Ag/CeO_2 catalyst with sodium doping might demonstrate in the forms of $NaHCO_3$ and Na_2CO_3, which could induce that surface hydroxyl (OH^-) concentrations increased markedly on the surface of CeO_2 nanospheres (Ma et al. 2018). The existing of sodium could prevent hydrogen spillover from Ag to CeO_2, indicating that the inhibiting effect of sodium shows in the process of reduction. For another example, Nie et al. (2013) investigated a successful alkali modification of Pt/TiO_2 catalyst owing to the formation of massive mesopores for the improvement of mass transfer and reaction kinetics, which was advantaged to improve catalytic oxidation of HCHO at room temperature. Furthermore, ceramic honeycombs with NaOH (Na-CH) modification were prepared by impregnating CH into NaOH aqueous solution (Yu et al. 2013). The enhanced performance of CH with NaOH modification obtained was attributed to the existence of NaOH and enhancement of surface areas and hydroxyl groups on the surface of these catalysts. Furthermore, nanoporous gold catalysts modified by alkali for CO oxidation were investigated and the results exhibited that hydroxyl ion adlayers (Au-OH-ads) produced can increase the activity (Han et al. 2011).

Herein, we reported a kind of sphere Bi_2WO_6 and Bi-TiO_2 with alkali-modification, as a kind of heterojunction structure in order to increase the efficiency of charge separation and decrease the recombination of photo-generated electrons and holes. In the meantime time, according to XRD, UV–Vis, FT-IR, and XPS, this paper figured out the processes of photocatalytic oxidation and mechanism, especially for the mixed catalysts with loading Na_2SO_4 exhibiting a high activity. Moreover, the stability of these catalysts was investigated and applied repetitively more than five times due to the favorable interaction of Bi_2WO_6 and $Bi_{0.15}Ti_{0.85}O_2$.

Experimental

Syntheses

The flower-like Bi-TiO_2 was prepared by a hydrothermal method (Huang et al., 2018a, b). In a typical synthesis, 41.4 mL of tetrabutyl titanate was added into a mixed solution A including an equal volume of ethanol and glycerol (24.3 mL). In addition, 9.3 g of Bi $(NO_3)_3$ was appended into a mixed solution B, which contained an equal volume of ethanol and glycerol (24.3 mL) and 19.2 mL of acetic acid, respectively. Under continuous stirring of solution A, the solution B was dropped into the solution A and then vigorously stirred for 30 min. The mixed solution was transferred into a Teflon-lined autoclave and heated at 110 °C for 48 h, and then it was taken out of the oven and cooled naturally. Afterward, these powders were collected with centrifugation and washed three times with ethanol. Finally, the powders of Bi-TiO_2 photocatalysts were dried at 80 °C for 4 h and calcined at 450 °C for 8.5 h. The sample of Bi-TiO_2 could be denoted as $Bi_{0.15}Ti_{0.85}O_2$ due to the molar ratio of Bi and Ti as 3:17.

The sphere of Bi_2WO_6 was synthesized by the hydrothermal method. $Na_2WO_4{\cdot}2H_2O$ (2.5 g) and 7.3 g of Bi $(NO_3)_3{\cdot}5H_2O$ were dropped into 60 mL deionized water respectively and kept stirring until completely dissolved. These two kinds of solution were mixed dropwise and kept stirring for another 30 min. And then, the solution was transferred into a Teflon-lined autoclave and heated at 180 °C for 12 h. After that, the yellow powders of samples were cooled and washed for three times until pH = 7.0. Then, the powders of Bi_2WO_6 were dried at 80 °C for 6 h. Finally, as for Bi_2WO_6 and $Bi_{0.15}Ti_{0.85}O_2$, these two kinds of powders were blended with according to a certain molar ratio and then ground into fine powders with dry conditions. The catalysts of Bi_2WO_6/TiO_2 and $Bi_2WO_6/Bi_{0.15}Ti_{0.85}O_2$ were denoted as D-BT and D-BBT, and the different molar ratios were identified as D-BT(1:4) and D-BBT(1:4).

In order to improve the activity of the mixed catalysts, the catalysts with alkali-modification were prepared with two different methods. One way was to append some alkali salts, such as NaOH, Na_2CO_3, Na_2SO_4, and K_2CO_3, into the D-BBT(1:4), which had been prepared before the appending of these alkali salts. The powders of D-BBT(1:4) were impregnated into these alkali salt solution for 2 h and then took out and calcinated at 450 °C for 2 h. The other way was to append these alkali salts into the solution for $Bi_{0.15}Ti_{0.85}O_2$ synthesizing, and then the $Bi_{0.15}Ti_{0.85}O_2$ with the dropping of alkali salts were dried at 80 °C for 4 h, calcined at 450 °C for 8.5 h, then mixed with Bi_2WO_6 together. These two kinds of catalysts were denoted as D-BBT(1:4)-NaOH, D-BBT-Na_2SO_4 (1:4), and so on.

Instead of dry mixing, a sample of BBT-Na_2SO_4 (1:4) was mixed with wet conditions in a solution, including an appropriate amount of Bi_2WO_6 and $Bi_{0.15}Ti_{0.85}O_2$ powders with Na_2SO_4 loading and identifying as W-BBT-Na_2SO_4 (1:4).

Characterizations

Powder X-ray diffraction of these catalysts were recorded by using a D/max-RB X-ray diffractometer equipped with Cu Kα radiation ($\lambda = 0.15406$ nm) in a 2θ range from 10 to 80° and the step size was 5°. BET surface areas were determined by using an automated gas sorption analyzer (Autosorb-iQ-AG-MP, Quantachrome Co., USA) with nitrogen adsorption at 77 K. These samples were all degassed at 300 °C for 2 h in a vacuum. The morphology of these catalysts was investigated using scanning electron microscopy (SEM, SU1510, Hitachi, Japan). The UV–Vis spectra were recorded by the Cary 100 UV–Vis spectrophotometer (Agilent, USA) with an integrating sphere attachment. The scanning range was from 200 to 800 nm, and $BaSO_4$ was used as a reference. The chemical binding energies of the Bi, Ti, O, Na, and S atoms were examined by X-ray photoelectron spectroscopy (XPS, ESCALAB250 Thermo VG, USA) using an Al Kα X-ray source (1486.6 eV) operated at 15 kV and 300 W. The infrared spectra (IR) were scanned in the range of 4000–600 cm^{-1} by using IR spectrometer (MAGNA-IR750, USA).

Activity measurements

Catalytic activities were measured on a self-designed glass reactor (600 × 600 × 600 mm). A certain amount of liquid formaldehyde was injected into the glass reactor with a microsyringe at dark, and then, the formaldehyde was volatilized. The concentration of formaldehyde was kept at a range of 1.05 ± 0.05 mg/m^3 at the beginning of the experiment and measured by Formaldehyde Meter (PPM-400ST, PPM Technology Ltd., England) from 0 to 12.28 mg/m^3. After that, 0.4 g of photocatalysts powers was laid into a culture dish evenly and then well placed at the bottom of the glass reactor under the LED light. The 36-W LED light was provided as the light source and was located 10 cm above these powders. The incident photon flux and average illumination on the surface of catalysts were 116 lm and 14,772 Lux, respectively, which was detected by using an illuminometer (Fluke 941, USA). And then, the energy-saving lamp was turned on and the formaldehyde concentration was measured at every 12 h. Degradation experiments were all carried out for 48 h at least. To investigate the activity of different catalysts, a set of gaseous experiments were carried out at room temperature.

Results and discussion

Catalyst characterization

Crystal structure

The phase and crystallographic structure of D-BT and D-BBT with Na_2SO_4 loading or different solutions mixing were investigated by using XRD. As shown in Fig. 1a, the diffraction peak from anatase TiO_2 (PDF no. 21-1272) was observed at 25.3° and 48.0° and increased with the increasing amount of TiO_2. Meanwhile, the diffraction peaks of Bi_2WO_6 (PDF no. 39-0256) were also detected at 28.3°, 32.8°, 47.1°, 56.0°, and 58.5°, but decreased with the decrease amount of Bi_2WO_6. Owing to TiO_2 with Bi_2O_3 doping in the D-BBT samples, the diffraction pattern from Bi_2O_3 and composite oxides of $Bi_2Ti_2O_7$ could be found. The composite oxides of $Bi_2Ti_2O_7$ and Bi_2O_3 were also beneficial to increase the separation of electron and hole and improving the activities of HCHO oxidation (Qian et al. 2017; Sood et al. 2016). Therefore, the samples of D-BBT exhibited higher activity than D-BT. As depicted in Fig. 1b, the catalysts prepared with Na_2SO_4 loading and different mixed solution were able to keep the crystallographic structure of Bi_2WO_6, TiO_2, and $Bi_2Ti_2O_7$, but the diffraction peak of Bi_2O_3 disappeared due to Na_2SO_4 increase the diffraction intensity of $Bi_2Ti_2O_7$ and Bi_2WO_6. In the meantime, a residual diffraction peak from Na_2SO_4 was observed at $2\theta = 32.1°$ (PDF no. 37-1465) in the samples of W-BBT-Na_2SO_4(1:4) mixed with the ethanol and sulfuric acids, while for D-BBT-Na_2SO_4(1:4), the crystallographic structure of Bi_2WO_6 disappeared owing to Na_2SO_4 loading and mechanical mixture. While adding increasing amount of Na_2SO_4 for W-BBT- Na_2SO_4(1:4) (Fig. 1c), the diffraction patterns did not change substantially and were similar to that of as-prepared W-BBT-Na_2SO_4(1:4)-water.

N_2 adsorption

The specific surface areas, average pore size, and total pore volume of Bi_2WO_6 and $Bi_{0.15}Ti_{0.85}O_2$ mixed catalysts are listed in Table 1. The surface areas, pore size, and pore volume of D-BBT increased with increasing the molar ratios of Bi_2WO_6 and $Bi_{0.15}Ti_{0.85}O_2$. Therefore, as for these catalysts, the D-BBT(1:4) showed the highest activity for HCHO oxidation with the highest surface areas. But for the W-BBT-Na_2SO_4(1:4) mixing with the different solutions, the S_{BET} and d_p increased in the W-BBT-Na_2SO_4(1:4)-sulfuric acid, while the volume decreased, possibly due to the corrosion of sulfuric acid and reacted with TiO_2 and Bi_2O_3. Therefore, the sample exhibited an extremely poor HCHO conversion probably due to this chemical reaction. As for W-BBT-Na_2SO_4 (1:4) with the different Na_2SO_4 loading amounts, the S_{BET}, d_p, and V were higher than the samples of D-BBT(1:4) attributed to solution mixture, which was beneficial to improve the activities. However, the S_{BET} would be firstly increased and then decreased with enhancing Na_2SO_4 loading and the sample with 2 wt% Na_2SO_4 showed the highest activity for HCHO oxidation with the highest surface areas, pore size, and pore volume probably due to the deposition of Na_2SO_4.

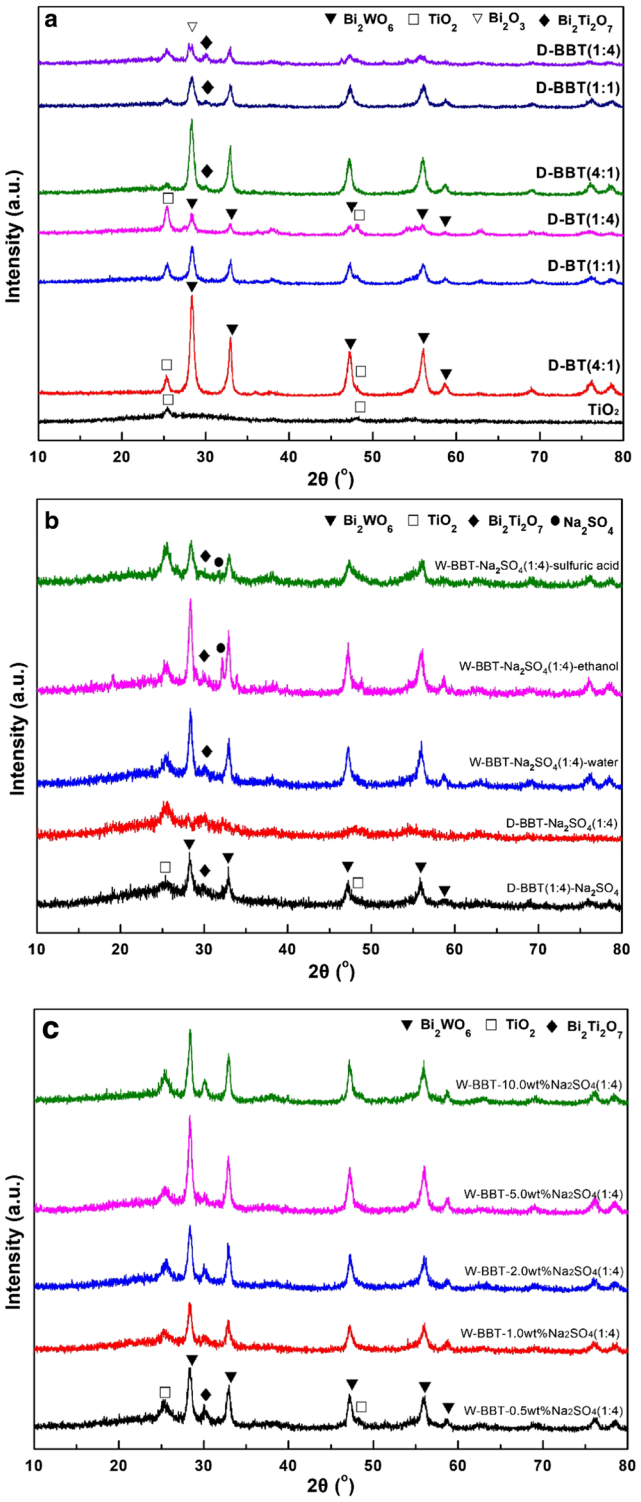

Fig. 1 XRD patterns of catalysts (**a** D-BT and D-BBT, **b** D-BBT-Na_2SO_4, and **c** W-BBT-Na_2SO_4 (1:4))

Table 1 The specific surface area (BET), average pore size (d_p), and total pore volume (V) of Bi_2WO_6 and $Bi_{0.15}Ti_{0.85}O_2$ mixed catalysts

Samples	BET (m^2/g)	d_p (cm^3/g)	V (nm)
D-BBT(4:1)	22.14	0.082	3.80
D-BBT(2:1)	25.71	0.087	3.80
D-BBT(1:1)	25.12	0.085	3.81
D-BBT(1:2)	32.80	0.095	3.83
D-BBT(1:4)	37.81	0.102	3.83
W-BBT-Na_2SO_4 (1:4)-water	32.03	0.10	4.81
W-BBT-Na_2SO_4 (1:4)-ethanol	23.00	0.074	5.19
W-BBT-Na_2SO_4 (1:4)-sulfuric acid	44.45	0.112	3.83
W-BBT-0.5wt%Na_2SO_4 (1:4)	50.95	0.114	5.18
W-BBT-1.0wt%Na_2SO_4 (1:4)	42.85	0.110	5.61
W-BBT-2.0wt%Na_2SO_4 (1:4)	57.15	0.122	5.65
W-BBT-5.0wt%Na_2SO_4 (1:4)	48.58	0.120	5.60
W-BBT-10.0wt%Na_2SO_4 (1:4)	44.26	0.110	5.63

Catalyst morphology

The microstructures and morphology of catalysts with alkali salt loading or solution mixing were investigated by using SEM. As shown in Fig. 2, the D-BBT(1:4)-Na_2SO_4 exhibited some mixed particles with spherical particles of Bi_2WO_6 and irregular particles and the size of spherical particles was about 8–10 μm. But the samples of D-BBT(1:4)-Na_2SO_4 (Fig. 2b) exhibited more sphere particles than D-BBT(1:4)-NaOH (Fig. 2a). The results indicated that the sodium hydroxide may react with Bi_2WO_6 and destroy the sphere structure. However, the D-BBT-Na_2SO_4(1:4) catalysts did not show any sphere particles and exhibited only a large number of irregular particles with rough surface due to dry mixed with a strong mechanical lapping, which was a disadvantage for defending the spherical particles of Bi_2WO_6. Owing to protect the structure, the dry mixed method was instead of wet mixed with water, ethanol, or sulfuric acid, and the results are exhibited in the Fig. 2d–f. From the results, three kinds of catalysts exhibited mixed particles with Bi_2WO_6 and their structure did not damage obviously. The SEM images of Fig. 2d exhibited highly dispersed particles consisting of spherical particles, and it was favorable to increase the oxidation activity for HCHO. However, compared with W-BBT-Na_2SO_4(1:4) with water, the sizes of these catalysts with the mixing of ethanol or sulfuric acid increased and the surface particles decomposed obviously for sulfuric acid owing to reaction with TiO_2 and Bi_2O_3. The samples, as shown in Fig. 2f, exhibited the high surface areas with corrosion, but the results indicated that the activity for HCHO oxidation decreased obviously. In addition, the water instead of ethanol was disadvantageous for improving the activity.

UV–visible absorption and PL spectra

The UV–Vis DRS spectra of D-BT, D-BBT, D-BBT(1:4)-alkali salts, D-BBT-alkali salts (1:4), and the band gaps of D-BBT with the different molar ratios of Bi_2WO_6 and $Bi_{0.15}Ti_{0.85}O_2$ are shown in Fig. 3a–d. Compared with pure TiO_2 (Yao et al. 2011), which was inactive owing to its big band gap (3.23 eV), the result demonstrated that D-BT samples showed a spectral response in visible areas due to the photosensitizing effect of Bi_2WO_6, which possibly owing to the multiple light reflections. The absorption edge of Bi_2WO_6 was identified as 464 nm (Ge and Liu 2011) attributed to the transition from the hybrid orbital of O 2p and Bi 6s to the W 5d orbital. However, accompanied by Bi_2O_3 doping, the absorption intensity of visible light for D-BBT samples was apparently increased with the increased amount of $Bi_{0.15}Ti_{0.85}O_2$ and a red shift appeared compared with D-BBT(4:1) samples owing to the enhanced number of surface Bi_2O_3 particles (Zhu et al. 2011). The enhancement of absorption with visible light should be attributed to the TiO_2 with Bi_2O_3 doping (Neppoliana et al. 2010). The band gap energies of D-BBT samples were confirmed from the plots of $(ahv)^2$ versus the energy of absorbed light. As shown in Fig. 3c, the estimated band gap values are approximately 2.80, 2.67, 2.60, 2.60, and 2.55 eV for D-BBT(4:1)~(1:4), respectively. Therefore, the activities increased with a large amount of $Bi_{0.15}Ti_{0.85}O_2$. More importantly, the D-BBT samples prepared with different methods and alkali salt loading, especially for Na_2SO_4, exhibited the diverse adsorption for visible light. As for Na_2SO_4 loading, the intensity of visible light absorption was higher than other samples, possibly due to sulfate (SO_4^{2-}), and it showed higher activity for HCHO oxidation. However, the UV–Vis DRS spectra of catalysts were almost the same as the different mixed solutions and loading amounts of Na_2SO_4.

The photoluminescence spectrogram (PL) displayed the photogenerated electrons and holes can be discovered under excitation, and these photogenerated electrons and holes may be recombined again with the releasing of fluorescence in the form of light energy. The intensity of fluorescence emission peak shows the recombination probability of these photogenerated electron and hole. As shown in Fig. 3e, the sample of W-BBT-Na_2SO_4(1:4) showed the lowest spectral intensity of fluorescence, indicating that the heterogeneous structure of W-BBT-Na_2SO_4(1:4) can effectively suppress the recombination of photogenerated electron and hole. The sample of Bi_2WO_6 displayed the highest, and D-BBT-Na2SO4 (1:4) was the second. Therefore, it could be speculated that the sample of W-BBT-Na_2SO_4(1:4) might be displayed the highest activity for HCHO oxidation, while the Bi_2WO_6 showed the lowest, which was consistent with the results of activities.

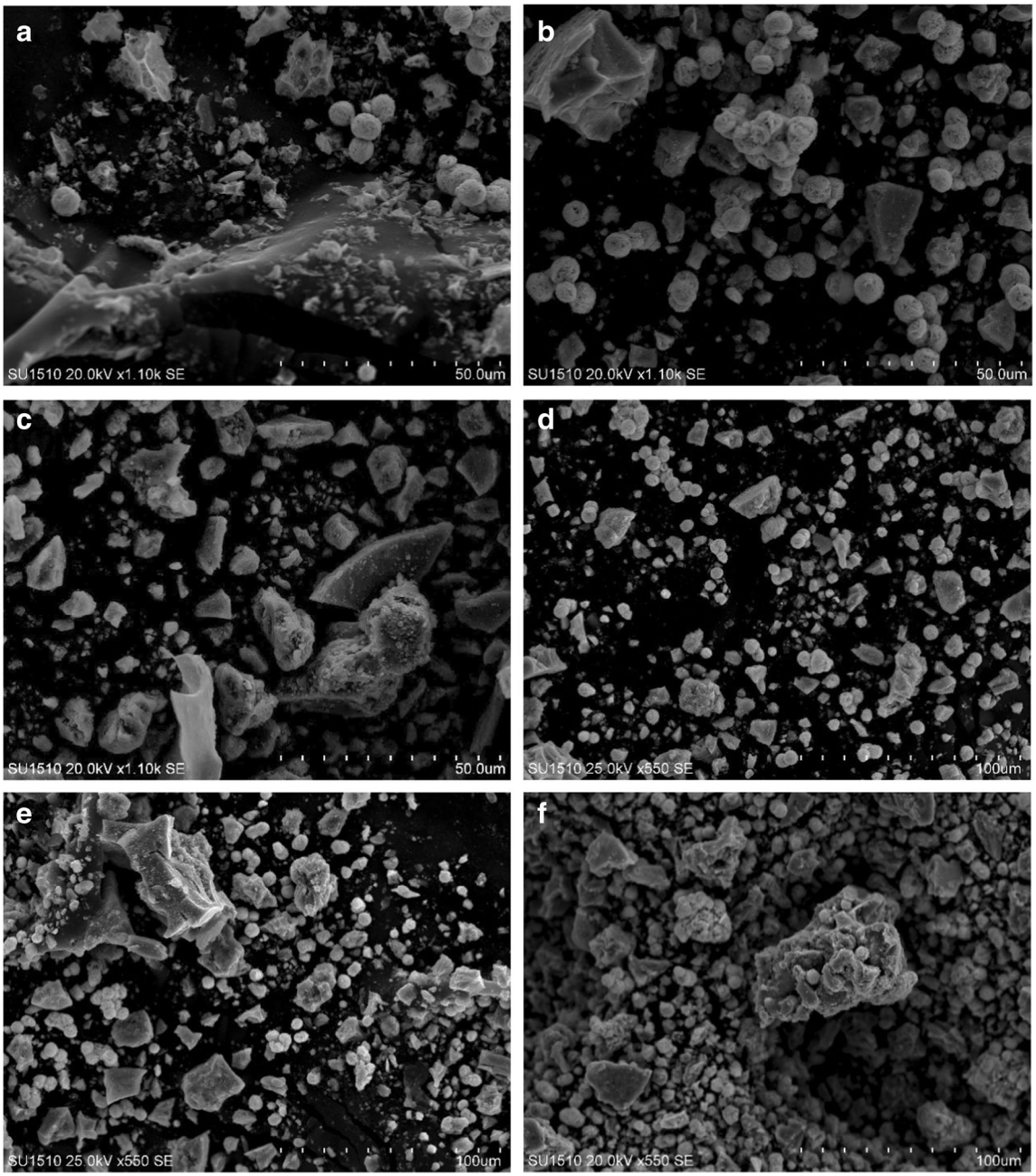

Fig. 2 SEM images of catalysts (**a** D-BBT(1:4)-NaOH, **b** D-BBT(1:4)-Na_2SO_4, **c** D-BBT-Na_2SO_4(1:4), **d** W-BBT-Na_2SO_4(1:4) with water, **e** W-BBT-Na_2SO_4(1:4) with ethanol and **f** W-BBT-Na_2SO_4(1:4) with sulfuric acid)

FT-IR spectrum

In order to further investigate the effect of alkali salt loading, FT-IR was applied to find the functional groups on the surface of these catalysts. As shown in Fig. 4, the broadbands around at 3385 cm^{-1} and 1624 cm^{-1} in all samples are attributed to the stretching vibration and bending vibration of the hydroxyl group from the adsorption of water (Liu et al. 2008). Moreover, it could be found that the performance of water adsorption varied obviously with the different alkali salt loading. Some researchers reported that loading of NaOH would graft extra surface OH^- groups (Yu et al. 2013; Zhang et al. 2012), but it was difficult to explain in the current experiment owing to these catalysts calcinated at 400 °C for 2 h. For D-BBT(1:4)-alkali salts (Fig. 4a), three absorption bands centered around 1375 cm^{-1}, 2906 cm^{-1}, and 2990 cm^{-1} correspond to the symmetric or different C–H orientations stretching vibration of formate (V_s (COO^-)) due to the inadequate oxidation of HCHO, especially for K_2CO_3. Therefore, they exhibited low activities for HCHO oxidation owing to the by-product as HCOOH. However, as shown in Fig. 4b, the weak peak at 1312 cm^{-1} was attributed to the stretching

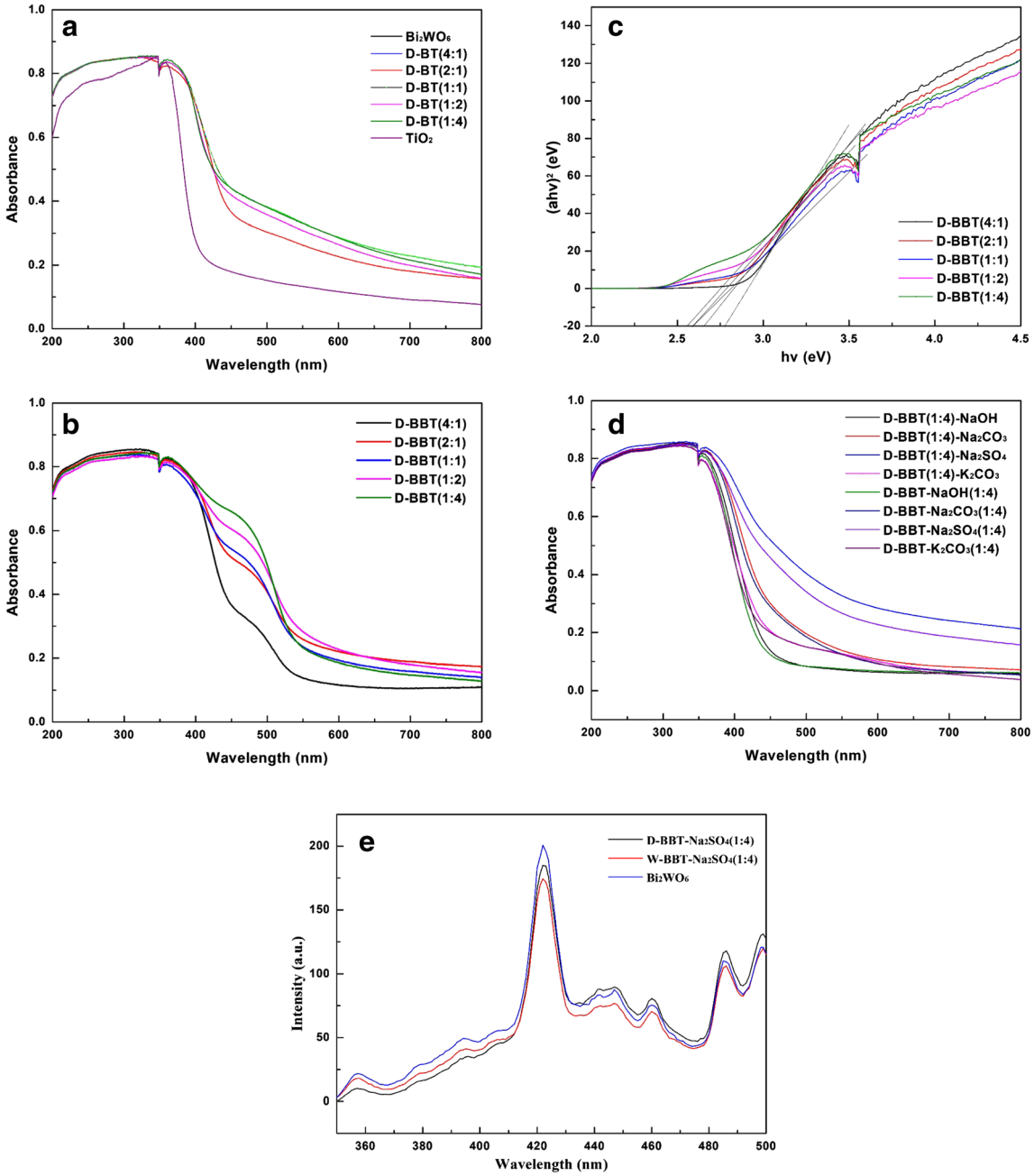

Fig. 3 UV–Vis DRS spectra, bands gaps and PL spectrogram of catalysts (**a** D-BT, **b**, **c** D-BBT, **d** D-BBT(1:4)-alkali salts and D-BBT-alkali salts (1:4), **e** W-BBT-Na_2SO_4(1:4))

vibration of C–O (ν CO_3^{2-}) due to the absorbing of carbonate or hydrocarbonate on the surface for D-BBT-alkali salts (1:4), particularly for Na_2CO_3, K_2CO_3, and NaOH loading. That was because that some oxidation products of carbon dioxide could be detected on the surface, so they exhibited a better activity than the samples as shown in Fig. 4a. Meanwhile, the catalyst with Na_2SO_4 loading could not find carbon dioxide due to the desorption with a larger amount of carbon dioxide, which showed higher activity than the other samples. From Fig. 4c, the broadband at 1127 cm^{-1} in Na_2SO_4 modification denoted to stretching vibration of sulfate (SO_4^{2-}) and the band firstly increased and then decreased with the of increase in Na_2SO_4. The results also denoted that these alkali salts were successfully doped into the catalysts and the functional groups on the surface were changed. It could not detect the stretching vibration of C-O (ν CO_3^{2-}) due to the high activity for HCHO oxidation.

XPS result

X-ray photoelectron spectroscopy (XPS) was utilized to investigate the chemical composition and states on the surface

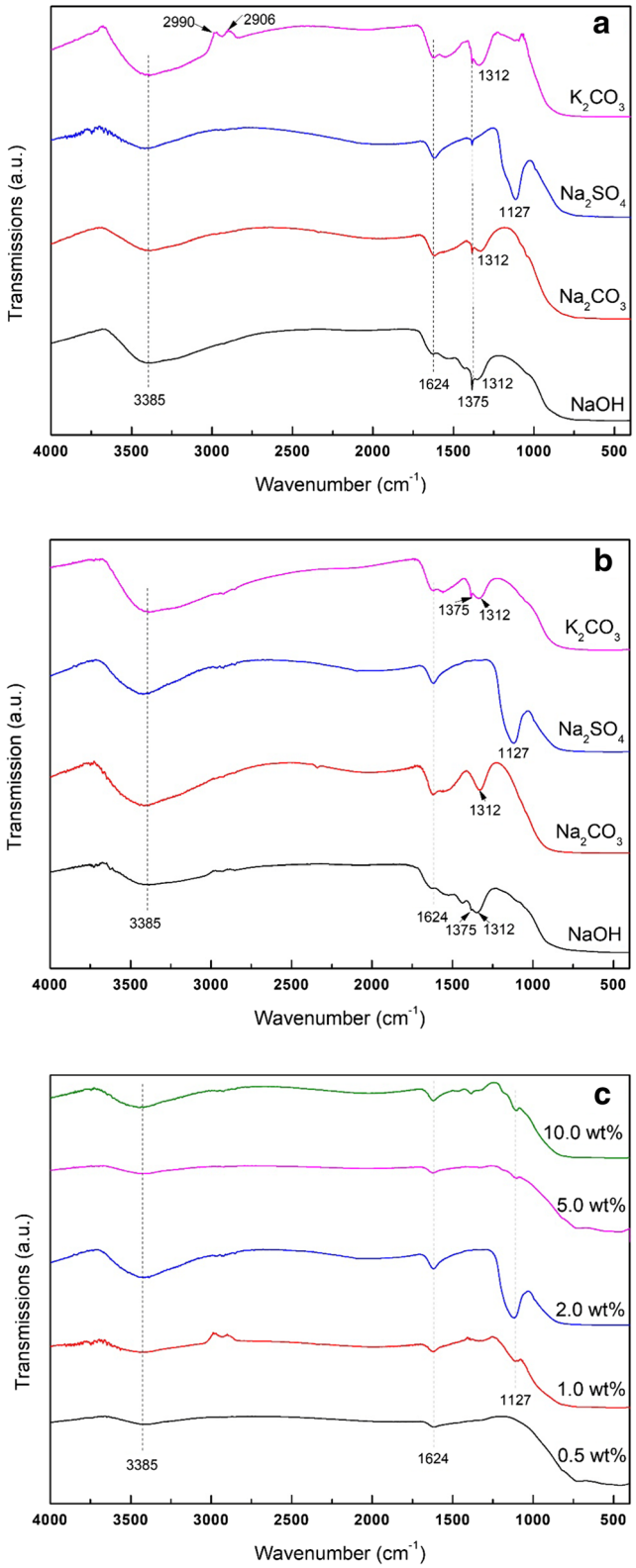

Fig. 4 FT-IR spectrum for catalysts (**a** D-BBT(1:4)-alkali salts, **b** D-BBT-alkali salts (1:4), and **c** W-BBT-Na_2SO_4 (1:4))

of catalysts. The XPS survey spectra in Fig. 5a identified that the catalysts were composed of Bi, Ti, W, O, Na, S, and a trace amount of C elements. As shown in Fig. 5b, the peaks at 159.1 eV and 164.4 eV were observed ascribed to Bi $4f_{7/2}$ and Bi $4f_{5/2}$, respectively (Liang et al. 2014). These two peaks were attributed to the Bi^{3+} species of Bi_2WO_6 and Bi_2O_3. In the meantime, the peaks for Bi^{3+} species did not change with the different mixed approaches of Bi_2WO_6 and $Bi_{0.15}Ti_{0.85}O_2$, even for alkali salt loading. The results indicated that the mixed approaches and alkali salt loading could not change the chemical states of Bi, the same for Ti. The XPS peaks in Fig. 5c were related to Ti 2p attributed to 458.7 eV (Ti $2p_{3/2}$) and 464.7 eV (Ti $2p_{1/2}$) (Liu et al. 2017), which is not in agreement with pure TiO_2 owing to Bi_2O_3 doping. As shown in Fig. 5d, it could be indicated that the O 1s peak of D-BBT(1:4)-Na_2SO_4 catalysts was deconvoluted into two symmetric Gaussian curves at peaks around 529.7 and 531.8 eV, which were ascribed to oxygen in the prepared sample lattice and surface-adsorbed oxygen, respectively (Zhou et al. 2015). The results indicated that the powders of D-BBT(1:4) modified with Na_2SO_4 were beneficial for the increasing of surface-adsorbed oxygen. While for the sample of W-BBT-2.0wt%Na_2SO_4 (1:4), it did not find the significant amounts of surface-adsorbed oxygen. The results demonstrated that the Na_2SO_4 dipped into the inner of $Bi_{0.15}Ti_{0.85}O_2$ and was not advantaged to adsorb oxygen in the air. The same results were as for the samples of D-BBT(1:4). Consequently, the peaks at 1072.2 eV (Fig. 2e) were attributed to the binding energies of Na 1s for Na^+ in the sample of D-BBT(1:4)-Na_2SO_4, which was consistent with the above results.

Catalytic activities

In all activity measurement, catalysts were subjected to a feed stream including 1.05 ± 0.05 mg/m^3 HCHO with a static air. As shown in Fig. 6a, these D-BT catalysts exhibited a low activity in HCHO degradation, obviously. However, as a result, it could be easily found that the activity of photocatalytic oxidation of HCHO increased with the growth of TiO_2 and the activities of these catalysts were mostly depended on TiO_2. Therefore, when the molar ratio was 1:4, the catalyst showed the highest conversion of HCHO among these catalysts. The concentration of HCHO was 0.348 mg/m^3 for 48 h, but it was still higher than the limitation of specification in China. However, the pure Bi_2WO_6 and TiO_2 were both exhibited a lower activity than the mixed samples. The results indicated that the enhanced photocatalytic effect of these mixed catalysts was attributed to the strong interaction between Bi_2WO_6 and TiO_2. From Fig. 6b, it can be found that the D-BBT catalysts exhibited a higher activity than the samples of D-BT (Fig. 6a). Moreover, the rate of HCHO degradation and the surface areas were enhanced simultaneously with the increasing amount of $Bi_{0.15}Ti_{0.85}O_2$. More importantly, the result was also confirmed that the photocatalytic activity was mainly depended on the $Bi_{0.15}Ti_{0.85}O_2$. The effect of Bi_2WO_6 may

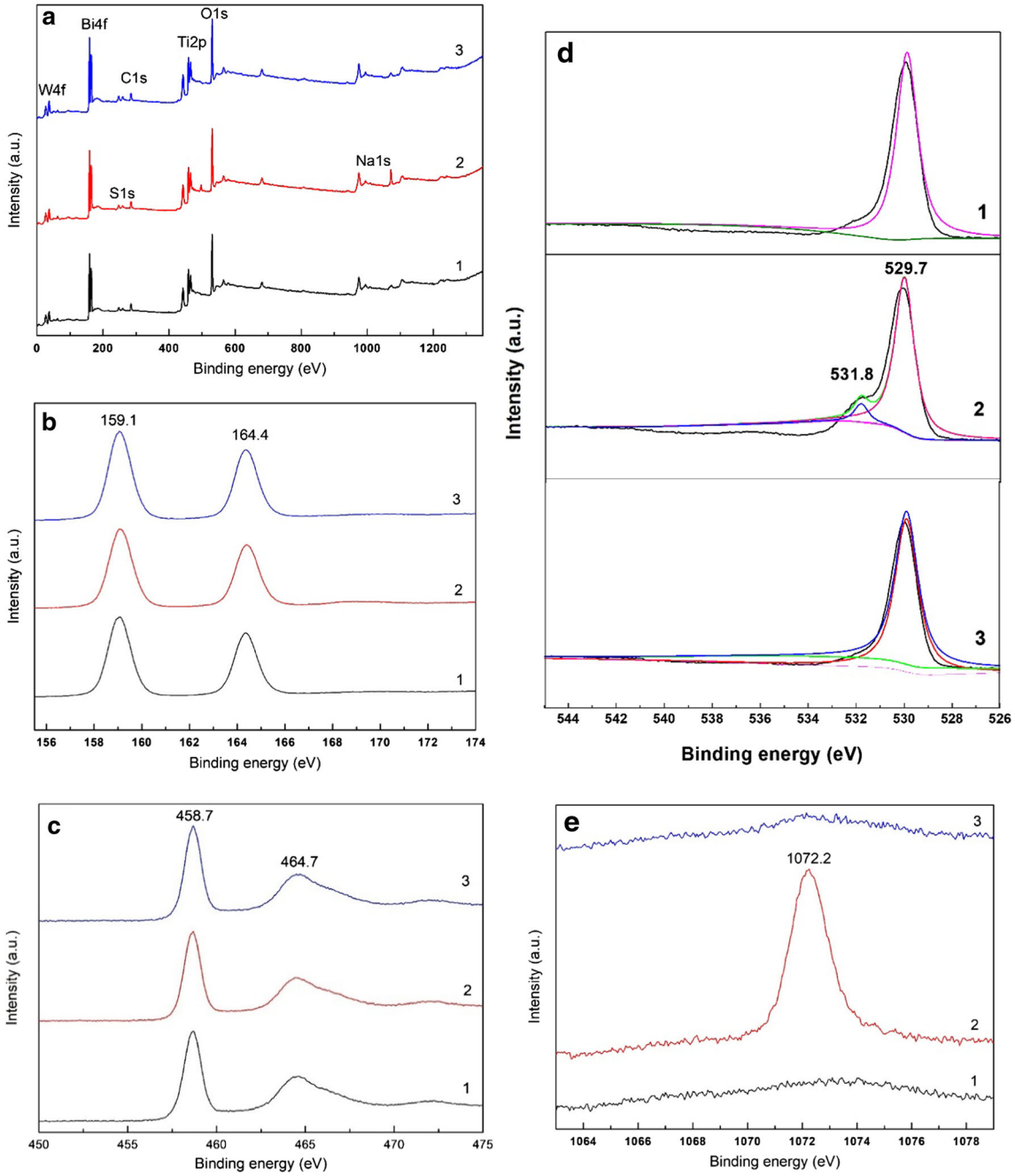

Fig. 5 XPS spectra of 1: D-BBT(1:4), 2: D-BBT(1:4)-Na_2SO_4 and 3: W-BBT-2.0wt%Na_2SO_4 (1:4): **a** survey, **b** Bi 4f, **c** Ti 2p, d O 1s, and **e** Na 1s

be assisted to improve the activity. Therefore, the D-BBT catalysts with the molar ratio at 1:4 exhibited the highest activity among these samples and the degradation rate of HCHO was 90.1% for 48 h. However, the pure $Bi_{0.15}Ti_{0.85}O_2$ catalysts exhibited a lower activity than D-BBT(1:4). The similarly synergistic effect between Bi_2WO_6 and $B_{i0.15}Ti_{0.85}O_2$ was exhibited in these mixed catalysts.

In order to further increase the photocatalytic activity, the best catalysts of D-BBT(1:4) were used to be modified. Meanwhile, it was well known that catalyst with alkali salt modification was a possible effective strategy to improve the activity for HCHO oxidation. Therefore, the catalysts with NaOH, Na_2CO_3, Na_2SO_4, and K_2CO_3 loading were investigated. The catalysts of D-BBT(1:4)-alkali salts and D-BBT-alkali salts (1:4) are exhibited in Fig. 7a, b, respectively. As shown in Fig. 7a, four types of alkali salt loading were all disadvantage for improving the activity for photocatalytic oxidation of HCHO due to the by-product of formic acid with the inadequate oxidation, which could be confirmed by FT-IR. Samples presented in Fig. 7b exhibited higher activity than samples in Fig. 7a due to the deep oxidation of formic acid to carbon dioxide. However, samples in Fig. 7b also showed

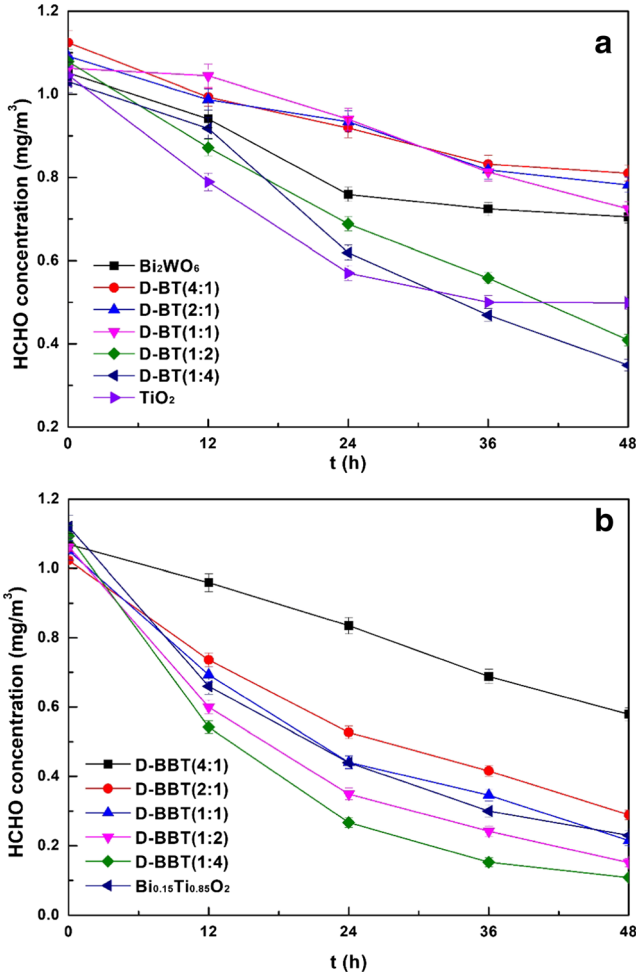

Fig. 6 Photocatalytic oxidation of HCHO over D-BT and D-BBT catalysts (HCHO concentration 1.05 ± 0.05 mg/m^3, catalyst amount 0.4 g, light source 36 W LED)

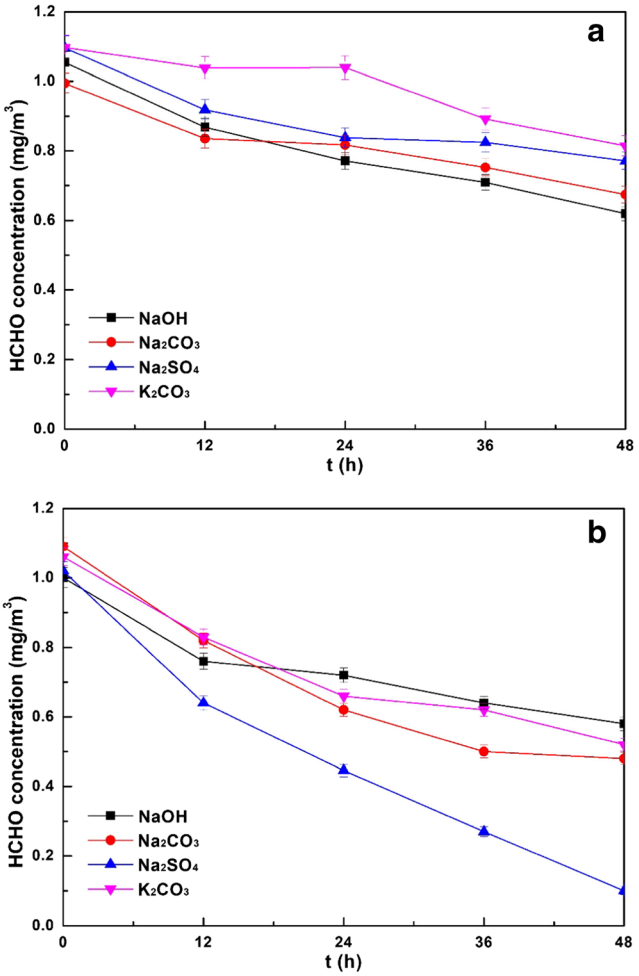

Fig. 7 Photocatalytic oxidation of HCHO over catalysts (A:D-BBT (1:4)-alkali salts and B: D-BBT-alkali salts (1:4)) (HCHO concentration 1.05 ± 0.05 mg/m^3, catalyst amount 0.4 g, light source 36 W LED)

low activities for HCHO oxidation, except for Na_2SO_4, which attributed to the desorption of carbon dioxide on the surface and more active sites. The results indicated that Na_2SO_4 offer more surface-adsorbed oxygen for deep oxidation of HCHO and promote the desorption of carbon dioxide, which was consistent with XPS.

In order to change the mixed method and further improve the activity, a simple mixed method by a mechanism was replaced by merging with the solution, including an appropriate amount of Bi_2WO_6 and $Bi_{0.15}Ti_{0.85}O_2$ powders with Na_2SO_4 loading. The results of W-BBT-Na_2SO_4 (1:4) with water, ethanol, or sulfuric acid (Fig. 8a) indicated that the liquid combining method was more favorable than the simple mechanical mixing to increase the activity for photocatalytic oxidation of HCHO. In these three kinds of solutions, the samples mixed with H_2O exhibited the largest activity for HCHO oxidation and the concentration of HCHO dropped from 1.09 to 0.10 mg/m^3 for 36 h due to the small size of $Bi_{0.15}Ti_{0.85}O_2$ particles (Fig. 3d). However, when the aqueous solution was replaced by ethanol or sulfuric acid, the W-BBT-Na_2SO_4 (1:4) catalysts with sulfuric acid showed a higher surface area than aqueous solution. This could be confirmed by BET and SEM. The activity for HCHO oxidation decreased. These results indicated that the specific surface area of catalysts was not the key to increase the activity for photocatalytic oxidation of HCHO.

The above results exhibited that Na_2SO_4 was advantageous to improve the performance, and so, the effects of increasing amounts of Na_2SO_4 were investigated and are exhibited in Fig. 8b. The specific surface areas of these catalysts decreased with the enhancing of Na_2SO_4, but the whole change was not obvious. For W-BBT-Na_2SO_4(1:4), it could be found that the activity was first decreased and then increased with the increasing amount of Na_2SO_4. When the loading amount was more than 2.0 wt%, the catalysts exhibited almost the same activity and the conversion of HCHO was 92.2% for 24 h, which was the best result and the concentration of HCHO was only 0.07 mg/m^3 below the limitation of specification in China.

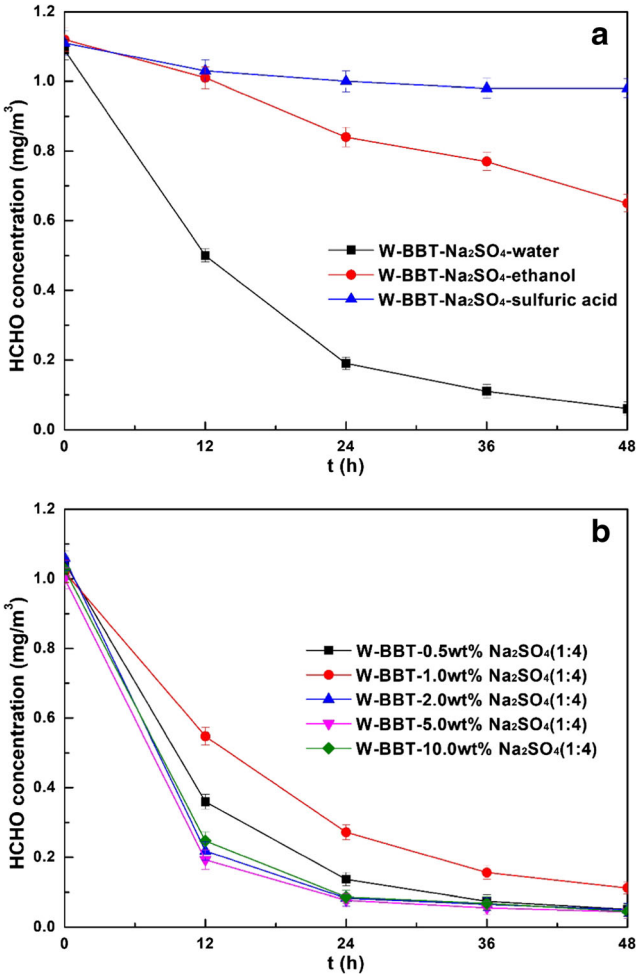

Fig. 8 Photocatalytic oxidation of HCHO over W-BBT-Na_2SO_4 (1:4) catalysts with the different solution and Na_2SO_4 amount (HCHO concentration 1.05 ± 0.05 mg/m^3, catalyst amount 0.4 g, light source 36 W LED)

Plausible mechanism

In view of the above results, a possible photocatalytic mechanism and oxidation process (Abdelraheem et al. 2016, Abdelraheem et al. 2019, Al-Anazia et al. 2018) for HCHO oxidation over $Bi_2WO_6/Bi_{0.15}Ti_{0.85}O_2$ catalysts was proposed to interpret the increased activity (Fig. 9). The E_{bg} for Bi_2O_3, TiO_2, and Bi_2WO_6 were about 2.70, 3.23, and 2.72 eV from UV–Vis DRS results, respectively. The equation was as follows (Sood et al. 2016):

$$E_{vb} = X – E_e + 0.5\, E_{bg}$$

E_{vb} Valence band edge potential
X Electronegativity of the semiconductor
E_e Energy of free electrons
E_{bg} Corresponding energy band gap
E_{cb} Conduction band edge potential

Based on the above equation, E_{cb} and E_{vb} of Bi_2O_3 were calculated as 0.065 eV and 2.835 eV, respectively. Meanwhile, the E_{cb} and E_{vb} of TiO_2 were calculated as − 0.25 eV and 2.98 eV, respectively. Further, the E_{cb} of TiO_2 was higher than that of the H^+/H_2 reduction potential. Because the E_{cb} of TiO_2 was more active than Bi_2O_3 (0.065 eV), the E_{cb} of TiO_2 was more active than Bi_2O_3. The different CB and VB cause a possible difference with the interface of these two semiconductors leading to the formation of heterojunction, same as Bi_2WO_6 and TiO_2. As a result, the photogenerated electron could be easily transferred from TiO_2 to Bi_2O_3. In the meantime, the holes migrated in the opposite direction, and the holes on the surface of Bi_2O_3 can easily move to TiO_2 through the interface. The formation of the heterojunction causes efficient charge separation leading to the effective reduction in the recombination of photo-generated electrons and holes. It is a simple generation of electrons and holes owing to hybridization of O (2p), Bi (6s), and Bi (6p) orbitals of Bi_2O_3, and the electrons could react with electron acceptors such as O_2, producing superoxide radical anion $\cdot O_2^-$ under visible light. Meanwhile, Bi_2WO_6 could be easily excited photogenerated electron and holes due to the narrow band gap energy. When the Bi_2WO_6 and TiO_2 were combined and applied as photocatalysts, electrons would transfer from the CB of Bi_2WO_6 to TiO_2 under visible light illumination due to the well-matched band level and the construction of tight heterogeneous interface, which effectively avoided the recombination of photogenerated electron and holes (Li et al. 2017). A plausible mechanism for photocatalytic degradation of HCHO over Bi_2WO_6/TiO_2 composite was proposed to interpret the increased photocatalytic activity, which showed in Fig. 9. Under visible light, Bi_2WO_6 with narrow band gap energy (2.72 eV) could be easily motivated and produced photogenerated electrons and holes, while TiO_2 could not be motivated due to its wide energy gap of 3.23 eV. When the Bi_2WO_6/TiO_2 composite was applied as photocatalysts for catalytic oxidation, photo-generated electrons will shift from the CB of Bi_2WO_6 to TiO_2 due to the well-matched band level and the construction of tight heterogeneous interface, which prevent the recombination of photogenerated charges, effectively. The separation of photogenerated electrons and holes in the Bi_2WO_6/TiO_2 heterostructure could be confirmed by PL emission spectra. What is more, the structure of TiO_2 with Bi_2O_3 doping exhibits excellent visible light scattering property, the scattering light overlaps with the absorption light of Bi_2WO_6, which can enhance the utility of incident light and produce more photoexcited electrons and holes. Hence, the photocatalytic efficiency as heterostructures was enhanced and complete degradation of HCHO took place. On the one hand, the alkali salts as Na_2SO_4, which could induce that surface hydroxyl (OH^-) concentrations markedly enhanced on the surface of these catalysts, could facilitate the partial adsorption of the by-product of HCOOH and CO_2. These

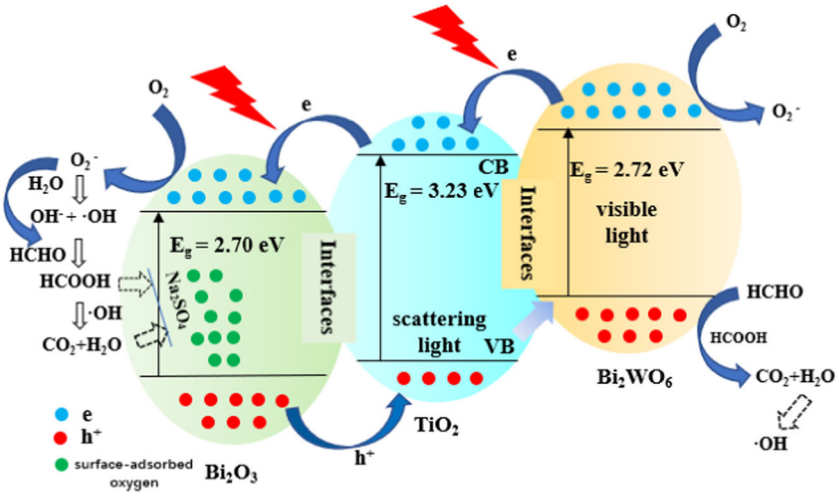

Fig. 9 Plausible mechanism over W-BBT-Na_2SO_4 (1:4) catalysts

surface hydroxyl groups were important reaction species and could react with adsorbed surface, as $HCOO^-$, to form H_2O and CO_2, directly. On the other hand, it could increase the amount of surface-adsorbed oxygen for catalytic oxidation of HCHO.

Stabilities of W-BBT-2.0%Na_2SO_4 (1:4)

The stability and efficiency are very important for these high activities of catalysts in applications. In order to investigate the stability of W-BBT-2.0%Na_2SO_4 (1:4) in HCHO oxidation, the oxidation reaction on photocatalytic decomposition of HCHO was repeated five times with 10 days and the results are exhibited in Fig. 10. The data demonstrated that the degradation rate of HCHO markedly decreased as compared with the result of fresh catalysts due to the adsorption of HCHO, especially in the first 12 h, but the final result for 48 h did not change indicating that the W-BBT-2.0%Na_2SO_4 (1:4) catalysts may keep a stable and efficient performance under visible light.

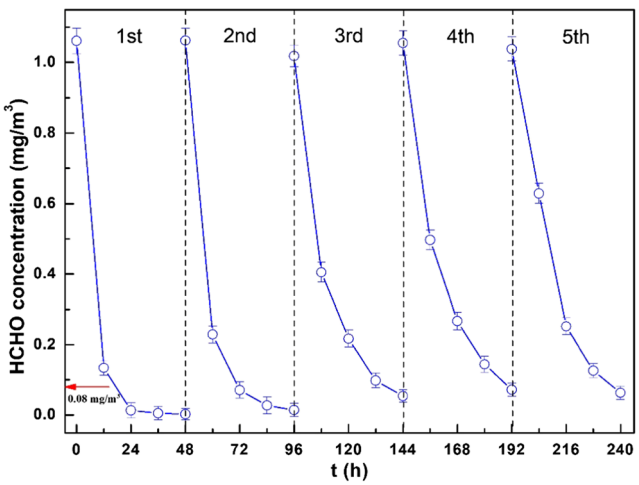

Fig. 10 The stability of photocatalytic oxidation of HCHO over W-BBT-2.0%Na_2SO_4 (1:4) catalysts (HCHO concentration 1.05 ± 0.05 mg/m^3, catalyst amount 0.4 g, light source 36 W LED)

Conclusions

This work demonstrates that the molar ratios of Bi_2WO_6 and $Bi_{0.15}Ti_{0.85}O_2$, mixed methods, and Na_2SO_4 loading all had the obvious promotion effect on HCHO oxidation over these mixed catalysts. The significant synergistic effects between Bi_2WO_6 and TiO_2, TiO_2, and Bi_2O_3 were exhibited in these mixed catalysts to improve the activity. The formation of two kinds of heterojunction causes efficient charge separation leading to the effective reduction in the recombination of photo-generated electrons and holes. The results also indicated that the liquid combining method instead by the mechanism mixing was more favorable to increase the HCHO conversion due to decrease the size of $Bi_{0.15}Ti_{0.85}O_2$ particles. Moreover, Na_2SO_4 loading to the catalysts led to more surface-adsorbed oxygen and facilitated the partial adsorption of the by-product of HCOOH and CO_2, which markedly increased the deep photocatalytic oxidation of HCHO. This work further demonstrated the promotion effect of Na_2SO_4, not for any alkali salts, on the activity for TiO_2 catalysts with metal oxide doping.

Funding information This work was financially supported by the Natural Science Foundation of Jiangsu Province (Nos. BK20170954 and BK20150890), the National Natural Science Foundation of China (Nos. 21501097), the Qing Lan Project of the Jiangsu Higher Education Institutions of China, the Priority Academic Program Development of Jiangsu Higher Education Institutions (PAPD), the Top-notch Academic Programs Project of Jiangsu Higher Education Institutions (PPZY2015C222), the Jiangsu Joint Laboratory of Atmospheric Pollution Control, and the Jiangsu Engineering Technology Research Centre of Environmental Cleaning Materials.

References

Abdelraheem WHM, Komy ZR, Ismail NM, Dionysiou DD (2016) Revealing the mechanism, pathways and kinetics of UV254nm/H_2O_2-based degradation of model active sunscreen ingredient PBSA. Chem Eng J 288:824–833

Abdelraheem WHM, Patil MK, Nadagouda MN, Dionysiou DD (2019) Hydrothermal synthesis of photoactive nitrogen-and boron-codoped TiO_2 nanoparticles for the treatment of bisphenol A in wastewater: synthesis, photocatalytic activity, degradation byproducts and reaction pathways. Appl Catal B Environ 241:598–611

Al-Anazia A, Abdelraheem WH, Han C, Nadagouda MN, Sygellou L, Arfanis MK, Falaras P, Sharma VK, Dionysiou DD (2018) Cobalt ferrite nanoparticles with controlled composition-peroxymonosulfate mediated degradation of 2-phenylbenzimidazole-5-sulfonic acid. Appl Catal B Environ 221:266–279

Carja G, Gilea D, Cool P, Seftel EM (2018) In situ synthesis of Bi_2O_3 nanoparticles on ZincMe (Me = Al or Cr) layered double hydroxide frameworks for photocatalytic oxygen evolution from water under solar-light activation. ChemCatChem 10:1598–1606

Cui PP, Hu Y, Zheng MM, Wei CH (2018) Enhancement of visible-light photocatalytic activities of $BiVO_4$ coupled with g-C_3N_4 prepared using different precursors. Environ Sci Pollut Res 25:32466–32477

Cui ZM, Yang H, Wang B, Li RS, Wang XX (2016) Effect of experimental parameters on the hydrothermal synthesis of Bi_2WO_6 nanostructures. Nanoscale Res Lett 11:190–199

Ge L, Liu J (2011) Efficient visible light-induced photocatalytic degradation of methyl orange by QDs sensitized CdS-Bi_2WO_6. Appl Catal B Environ 105(3–4):289–297

Han DQ, Zhou CQ, Yin HM, Zhang DJ, Xu XH (2011) Reactivity of the alkaline pretreated nanoporous gold for the CO oxidation. Catal Lett 141:1026–1031

He RG, Xu DF, Cheng B, Yu JG, Ho WK (2018a) Review on nanoscale Bi-based photocatalysts. Nanoscale Horizons 3:464–504

He RG, Zhou JQ, Fu HQ, Zhang SY, Jiang CJ (2018b) Room-temperature in situ fabrication of Bi_2O_3/g-C_3N_4 direct Z-scheme photocatalyst with enhanced photocatalytic activity. Appl Surf Sci 430:273–282

Hu Y, Cao YT, Wang PX, Li DZ, Chen W, He YH, Fu XZ, Shao Y, Zheng Y (2012) A new perspective for effect of Bi on the photocatalytic activity of Bi-doped TiO_2. Appl Catal B Environ 125:294–303

Huang TT, Li YH, Wu XF, Lv KL, Li Q, Li M, Du DY, Ye HP (2018a) In-situ transformation of Bi_2WO_6 to highly photoreactive Bi_2WO_6@Bi_2S_3 nanoplate via ion exchange. Chin J Catal 39:718–727

Huang Q, Wang Q, Tao T, Zhao YX, Wang P, Ding ZY, Chen MD (2018b) Controlled synthesis of Bi_2O_3/TiO_2 catalysts with mixed alcohols for the photocatalytic oxidation of HCHO. Environ Technol:1:1–1:111

Huang YF, Wei YL, Wang J, Luo D, Fan LQ, Wu JH (2017) Controllable fabrication of Bi_2O_3/TiO_2 heterojunction with excellent visible-light responsive photocatalytic performance. Appl Surf Sci 423:119–130

Huang YK, Kang SF, Yang Y, Qin HF, Ni ZJ, Yang SJ, Li X (2016) Facile synthesis of Bi/Bi_2WO_6 nanocomposite with enhanced photocatalytic activity under visible light. Appl Catal B Environ 196:89–99

Hwang YJ, Yang S, Lee H (2017) Surface analysis of N-doped TiO_2 nanorods and their enhanced photocatalytic oxidation activity. Appl Catal B Environ 204:209–215

Li B, Chen XW, Zhang TY, Jiang S, Zhang GH, Wu WB, Ma XY (2018) Photocatalytic selective hydroxylation of phenol to dihydroxybenzene by BiOI/TiO_2 p-n heterojunction photocatalysts for enhanced photocatalytic activity. Appl Surf Sci 439:1047–1056

Li H, Zhang TX, Pan C, Pu CC, Hu Y, Hu XY, Liu EZ, Fan J (2017) Self-assembled Bi_2MoO_6/TiO_2 nanofiber heterojunction film with enhanced photocatalytic activities. Appl Surf Sci 391:303–310

Li XX, Fang SM, Ge L, Han CC, Qiu P, Liu WL (2015) Synthesis of flower-like Ag/AgCl-Bi_2MoO_6 plasmonic photocatalysts with enhanced visible-light photocatalytic performance. Appl Catal B Environ 176–177:62–69

Liang J, Zhu GQ, Liu P, Luo XC, Tan CW, Jin L, Zhou JP (2014) Synthesis and characterization of Fe-doped-Bi_2O_3 porous microspheres with enhanced visible light photocatalytic activity. Superlattice Microst 72:272–282

Liu TX, Li FB, Li XZ (2008) TiO_2 hydrosols with high activity for photocatalytic degradation of formaldehyde in a gaseous phase. J Hazard Mater 152:347–355

Liu Y, Wei B, Xu LL, Gao H, Zhang MY (2015) Generation of oxygen vacancy and OH radicals: a comparative study of Bi_2WO_6 and Bi_2WO_{6-x} nanoplates. ChemCatChem 7(24):4076–4084

Liu YB, Zhu GQ, Gao JZ, Hojamberdiev M, Zhu RL, Wei XM, Guo QM, Liu P (2017) Enhanced photocatalytic activity of $Bi_4Ti_3O_{12}$ nanosheets by Fe^{3+}-doping and the addition of Au nanoparticles: photodegradation of phenol and bisphenol A. Appl Catal B Environ 200:72–82

Liu YD, Xin F, Wang FM, Luo SX, Yin XH (2010) Synthesis, characterization, and activities of visible light-driven Bi_2O_3–TiO_2 composite photocatalysts [J]. J Alloys Compd 498(2):179–184

Low JX, Yu JG, Jsroniec M, Wageh S, Al-Ghanmdi AA (2017) Heterojunction photocatalysts. Adv Mater 29:1601694–1601714

Lucky RA, Charpentier PA (2010) N-doped ZrO_2/TiO_2 bimetallic materials synthesized in supercritical CO_2: morphology and photocatalytic activity. Appl Catal B Environ 96:516–523

Ma L, Seo CY, Chen XY, Li JH, Schwank JW (2018) Sodium-promoted Ag/CeO_2 nanospheres for catalytic oxidation of formaldehyde. Chem Eng J 350:419–428

Mattsson A, Lejon C, Bakardjieva S, Stengl V, Osterlund L (2013) Characterisation, phase stability and surface chemical properties of photocatalytic active Zr and Y co-doped anatase TiO_2 nanoparticles. J Solid State Chem 199:212–223

Neppoliana B, Kima Y, Ashokkumarc M, Yamashitab H, Choi H (2010) Preparation and properties of visible light responsive $ZrTiO_4$/Bi_2O_3 photocatalysts for 4-chlorophenol decomposition. J Hazard Mater 182:557–562

Nie LH, Yu JG, Li XY, Cheng B, Liu G, Jaroniec M (2013) Enhanced performance of NaOH-modified Pt/TiO_2 toward room temperature selective oxidation of formaldehyde. Environ Sci Technol 47:2777–2783

Portela R, Jansson I, Suárez S, Villarroel M, Sánchez B, Avila P (2017) Natural silicate-TiO_2 hybrids for photocatalytic oxidation of formaldehyde in gas phase. Chem Eng J 310:560–570

Qian K, Xia L, Wei W, Chen LL, Jiang ZF, Jing JJ, Xie JM (2017) Construction of $Bi_2Ti_2O_7$/$Bi_4Ti_3O_{12}$ composites with enhanced visible light photocatalytic activity. Mater Lett 206:245–248

Sanz O, Delgado JJ, Navarro P, Arzamendi G, Gandía LM, Montes M (2011) VOCs combustion catalyzed by platinum supported on manganese octahedral molecular sieves. Appl Catal B Environ 110:231–237

Shayegan Z, Lee CS, Haghighat F (2018) TiO_2 photocatalyst for removal of volatile organic compounds in gas phase—a review. Chem Eng J 334:2408–2439

Sood S, Mehta SK, Sinha ASK, Kansal SK (2016) Bi_2O_3/TiO_2 heterostructures: synthesis, characterization and their application in solar light mediated photocatalyzed degradation of an antibiotic, ofloxacin. Chem Eng J 290:45–52

Sun YJ, Xiao X, Dong XN, Dong F, Zhang W (2017) Heterostructured BiOI@La (OH)3 nanorods with enhanced visible light photocatalytic NO removal. Chin J Catal 38:217–226

Tian N, Zhang YH, Huang HW, He Y, Guo YX (2014) Influences of Gd substitution on the crystal structure and visible light-driven photocatalytic performance of Bi_2WO_6. J Phys Chem C 118(29):15640–15648

Tian J, Sang YH, Yu GW, Jiang HD, Mu XN, Liu H (2013) A Bi_2WO_6-based hybrid photocatalyst with broad spectrum photocatalytic properties under UV, visible, and near-infrared irradiation. Adv Mater 25:5075–5080

Topka P, Klementova M (2016) Total oxidation of ethanol over Au/$Ce_{0.5}Z_{r0.5}O_2$ cordierite monolithic catalysts. Appl Catal A Gen 522:130–137

Wang DJ, Guo L, Zhen YZ, Yue LL, Xue GL, Fu F (2014) AgBr quantum dots decorated mesoporous Bi_2WO_6 architectures with enhanced photocatalytic activities for methylene blue. J Mater Chem A 2: 11716–11727

Wang RS, Li BX, Xiao Y, Tao XQ, Su XT, Dong XP (2018) Optimizing Pd and Au-Pd decorated Bi_2WO_6 ultrathin nanosheets for photocatalytic selective oxidation of aromatic alcohols. J Catal 364:154–165

Wang W, Lu CH, Ni YR, Su MX, Xu ZZ (2012) Hydrothermal synthesis and enhanced photocatalytic activity of flower-like TiO_2 on carbon nanotubes. Mater Lett 79:11–13

Wang XJ, Chang LL, Wang JR, Song NN, Liu HL, Wan XL (2013) Facile hydrothermal synthesis of Bi_2WO_6 microdiscs with enhanced photocatalytic activity. Appl Surf Sci 270:685–689

Xia JX, Di J, Yin S, Xu H, Zhang J, Xu YG, Xu L, Li HM, Ji MX (2014) Facile fabrication of the visible-light-driven Bi_2WO_6/BiOBr composite with enhanced photocatalytic activity. RSC Adv 4:82–90

Yan PP, Li D, Ma XG, Xue JQ, Zhang YJ, Liu MB (2018) Hydrothermal synthesis of Bi_2WO_6 with a new tungsten source and enhanced photocatalytic activity of Bi2WO6 hybridized with C_3N_4. Photochem Photobiol Sci 17:1084–1090

Yang H (2014) China must continue the momentum of green law. Nature 509:535–535

Yang H, Flower RJ, Thompson JR (2018a) Identify and punish ozone depleters. Nature 560:167–167

Yang H, Ma M, Thompson JR, Flower RJ (2018b) Waste management, informal recycling, environmental pollution and public health. J Epidemiol Community Health 72:237–243

Yang JJ, Li DX, Zhang ZJ, Li QL, Wang HQ (2000) A study of the photocatalytic oxidation of formaldehyde on Pt/Fe_2O_3/TiO_2. J Photochem Photobiol A Chem 137(2–3):197–202

Yang YQ, Yin LC, Gong Y, Niu P, Wang JQ, Gu L, Chen XQ, Liu G, Wang LZ, Cheng HM (2018c) An unusual strong visible-light absorption band in red anatase TiO2 photocatalyst induced by atomic hydrogen-occupied oxygen vacancies. Adv Mater 30:1704479–1704487

Yao XJ, Wang XD, Su L, Yan H, Yao M (2011) Band structure and photocatalytic properties of N/Zr co-doped anatase TiO_2 from first-principles study [J]. J Mol Catal A Chem 351:11–16

Yu CF, Yang PY, Tie LN, Yang SY, Dong SY, Sun JY, Sun JH (2018) One-pot fabrication of b-Bi2O3@Bi2S3 hierarchical hollow spheres with advanced sunlight photocatalytic RhB oxidation and Cr (VI) reduction activities. Appl Surf Sci 455:8–17

Yu JG, Li XY, Xu ZH, Xiao W (2013) NaOH-modified ceramic honeycomb with enhanced formaldehyde adsorption and removal performance. Environ Sci Technol 47:9928–9933

Zhang CB, Liu FD, Zhai YP, Ariga H, Yi N, Liu YC, Asakura K, Flytzani-Stephanopoulos M, He H (2012) Alkali-metal-promoted Pt/TiO_2 opens a more efficient pathway to formaldehyde oxidation at ambient temperatures. Angew Chem Int Ed 51:9628–9632

Zhang G, Hu ZY, Sun M, Liu Y, Liu LM, Liu HJ, Huang CP, Qu JH, Li JH (2015) Formation of Bi_2WO_6 bipyramids with vacancy pairs for enhanced solar-driven photoactivity. Adv Funct Mater 25:3726–3734

Zhang L, Ghimire P, Phuriragpitikhon J, Jiang B, Goncalves AAS, Jaroniec M (2018) Facile formation of metallic bismuth/bismuth oxide heterojunction on porous carbon with enhanced photocatalytic activity. J Colloid Interface Sci 513:82–91

Zhou YG, Zhang YF, Lin MS, Long JL, Zhang ZZ, Lin HX, Wu JCS, Wang XX (2015) Monolayered Bi_2WO_6 nanosheets mimicking heterojunction interface with open surfaces for photocatalysis. Nat Commun 6:8340–8348

Zhu J, Wang SH, Wang JG, Zhang DQ, Li HX (2011) Highly active and durable Bi_2O_3/TiO_2 visible photocatalyst in flower-like spheres with surface-enriched Bi_2O_3 quantum dots. Appl Catal B Environ 102: 120–125

Zhu MP, Muhammad Y, Hu P, Wang BF, Wu Y, Sun XD, Tong ZF, Zhao ZX (2018) Enhanced interfacial contact of dopamine bridged melamine-graphene/TiO_2 nano-capsules for efficient photocatalytic degradation of gaseous formaldehyde. Appl Catal B Environ 232:182–193